An Inkjet-Printed Paper-Based Flexible Sensor for Pressure Mapping Applications

Steven D. Gardner*, J. Iwan D. Alexander*, Yehia Massoud†, and Mohammad R. Haider*
*School of Engineering, University of Alabama at Birmingham, Birmingham, AL, USA
†School of Systems and Enterprises, Stevens Institute of Technology, Hoboken, NJ, USA
{stevendg, ialex, mrhaider}@uab.edu, ymassoud@stevens.edu

***Abstract*—Biometric observation using portable and wearable sensors is transforming health monitoring since patients can now have their conditions frequently checked outside the hospital setting. However, modern biosensors mostly use the standard printed circuit board substrate, which is physically incompatible with irregular-surface applications. The need for a flexible, low-cost and high-resolution monitoring device for observing elderly patient mobility out of hospital settings is the motivation driving this research. The following paper is a characterization of an experimental inkjet-printed sensor that circumvents the problem of rigidity by using a highly flexible substrate while also benefiting from low fabrication costs, low power usage, and environmental friendliness. The sensor is a 4×4 grid of Aluminum-doped Zinc Oxide nodes inkjet-printed on paper-based substrates. The tests performed show nodes are capable of responding to applied pressures of over 540 PSI. Notably, they exhibit sensitivity to heat and humidity without shielding measures, making it more useful for physical therapy. Power usage of the device is shown to be as low as 5 μW. Silver nanoparticle ink was chosen as electrical routing between the Zinc Oxide and data collection scheme. The analog signal is connected through ELVIS II+ analog pins, where a MATLAB script retrieves and stores the data for visual analysis. The cost of printing a single pressure node of this sensor is estimated to be $0.01. These conditions make it a monetarily attractive pressure sensing and mapping option for human impact monitoring applications.**

***Index Terms*—biometric sensor, AZO, pressure gauge, inkjet-printed sensor**

I. Introduction

Pressure sensing is a critical parameter to observe in healthcare for patients undergoing physical therapy, those with physically high-risk jobs (e.g. construction workers, sports players, tower maintenance, etc.), and populations with delicate health as often seen in the elderly community. Thus, a pressure sensor that maintains flexibility with a minimal profile is a desirable technology and the motivation behind this work.

Inkjet-printed sensors is a promising approach due to ultra-low fabrication/setup costs, environmental friendliness, fast print times, flexibility for irregular surfaces and rich variety of sensor applications. Hazardous chemicals or scrap metal byproducts seen from etching in printed circuit boards (PCBs) are entirely avoided [1], [2]. Many materials such as the nanoparticle inks and paper-based substrates are biodegradable. The time from design to fabrication for a page of sensors may be only a couple of hours, making reprints from revised circuits quick and easy.

There are shortfalls of inkjet-printed circuits that prevent them from being largely commercialized. The print quality of drop-on-demand printers is variable between samples due to ink viscosity, material interaction and uneven curing [3]–[5]. Layering is an issue since there is no complete uniformity from printing. The gate bleeds through the insulating layer, shorting with the semiconductor. Another limitation is with the variety of commercially available nanoparticle inks. For instance, Millipore-Sigma is limited to carbon nanotubes (CNTs), graphene (GN), PEDOT:PSS, boron nitride (hBN), Aluminum-doped Zinc Oxide (AZO) and silver (Ag). The semiconductors' properties, barring some forms of graphene, are depletion-mode materials (p-type) and thus cannot achieve complimentary pairs for logic gates or higher forms of computation like arithmetic logic units [6], [7]. Some n-type materials are being researched but have not reached the market. Additionally, paper substrates are sensitive to environmental conditions such as oxygen, humidity and temperature. These limitations make reliability and repeatability a challenge.

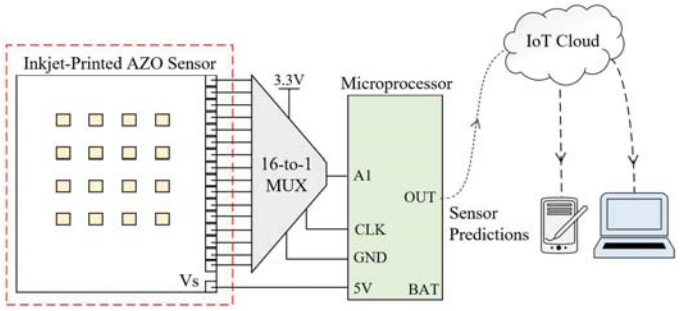

Fig. 1: Conceptual diagram of a system-level data processing scheme for usage as a commercialized, IoT-connected sensor device.

The printed sensor characterized in this report is conceptually shown as input to a system-level data acquisition scheme in Fig. 1. The sensor consists of a silver pattern with Aluminum-doped Zinc Oxide forming the active region. Zinc Oxide is a well known piezoelectric material [8]–[10]. Its conductivity increases when a deformation of its lattice takes place. This makes it particularly useful as a strain gauge, and especially useful when manufactured via thin-film deposition as many researchers have pursued [11]–[15]. Lately, Zinc Oxide has been used as a photosensitive applications [16], [17]. The goal of this research is to establish the metrics of this sensor such that there is evidence supporting its application to a system-level design. The applications of this is most

notably a cost-effective pressure mapping sensor for mobility [18], [19]. However, the sensor may be used for impact assessment of high-risk jobs (e.g. contact sports, construction, physical therapy, etc.). The charging/discharging effect of the temperature exposures to AZO and the paper-based substrate make this sensor also useful for mapping small temperature-specific events such as the growth of incubated bacteria cultures.

The organization of the paper is as follows. The inkjet-printed, AZO sensor array fabrication is elaborated in section II. Section III explores the various behaviors and characterizations of the device for usage in a system-level scheme. Lastly, section IV summarizes findings from the test results with a look into what is next for this research.

II. AZO Pressure Sensor Array Materials, Fabrication and Testing Equipment

The sensor is printed, cured and tested in the BioInspired Integrated Circuits (https://sites.uab.edu/mrhaider/) laboratory at the University of Alabama Birmingham. The nanoparticle inks are from Millipore-Sigma and Mitzubishi Paper Mills Inc. Aluminum-doped ZnO (model 901065) was ordered from the former and silver nanoparticle ink (model NBSIJ-MU01) from the latter. Ink is printed onto the glossy photopaper substrate using a Brother MFC-J5910DW inkjet printer containing the nanoparticles. The sensor in this report is made by printing the semiconducting layer and feeding the paper back through for the conductive layer (Fig. 2). The area of each node as seen in Fig. 2 is 0.0259 in^2. After printing, the circuit cures on a hotplate at 160 ^{o}C for 15 minutes [20].

The nature of a pressure sensor is that physical contact is being made with the material and nanoparticles are removed/damaged if anything brushes against them. Thus, these sensors are meant to be used once and discarded. However, based on an approximation of ink used per sensor, the cost comes out to only about $0.01 per node so the monetary impact of its usage is minimal. Tests were performed using a Keithley 2604B Dual SourceMeter, MATLAB and the NI ELVIS II+ prototyping board.

III. Single Node Behavior and Metrics

A single node, as seen in the image of Fig. 2, was tested to understand its behavior before exploring the entire pressure array. An overview of a single node's general functions, and its linear relationship between supply voltage and output

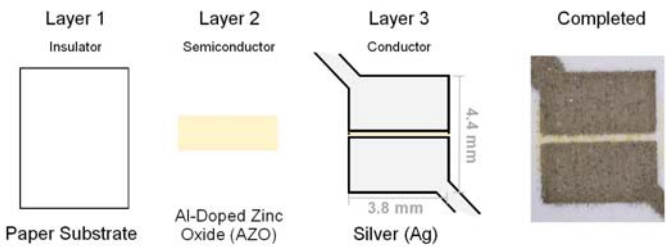

Fig. 2: Three layers of the printed array required to fabricate the sensor.

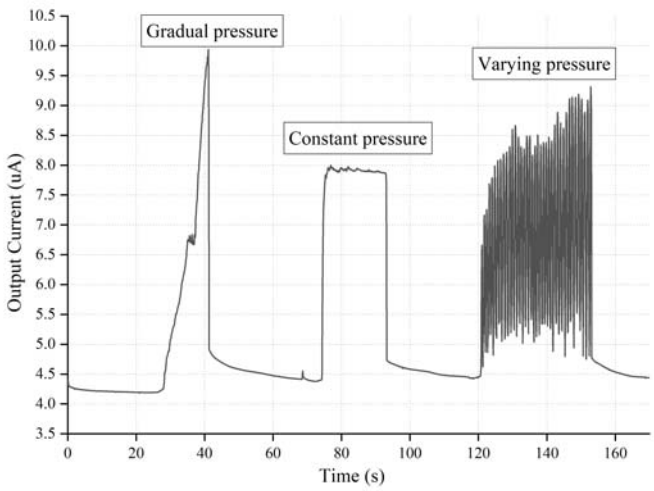

Fig. 3: Current output response when various pressure profiles are applied to node a_{11}.

current was shown in [18]. The response from the I-V curves of Fig. 6 show that the supply voltage may be reduced to 5V for an output of about 1 μA (5 μW of power). Channel resistance due to the conductivity of AZO as a single printed layer causes the node resistance to be in the mega-ohm range in its unused state. As pressure is applied, the resistance decreases dramatically. Fig. 4 shows the sensor's response from various pressure profiles applied with the finger. It is clear that nodes of this printed array are highly sensitive to gradual, constant and chaotic pressure changes by human contact. This report characterizes its behavior further such that it may be refined and applied to system-level designs.

1) Sensor Behavior: Since the previous study, testing has indicated that the sensor is highly responsive to heat and humidity, helping to explain its behavior. Electron mobility

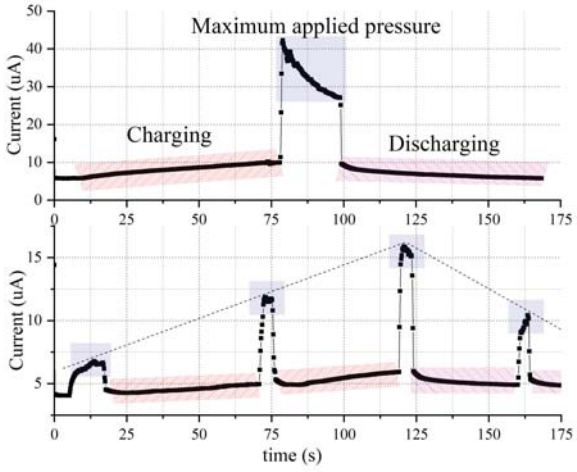

Fig. 4: Closer look at the effect of charging on the output current using pressure applied with the index finger. Charging occurs by hovering the finger a distance of 1 mm from the node. Nodes are a_{44} (top) and a_{14} (bottom). Vsupply = 20 V.

across the node slowly increases when a heat source is within 4 mm from the surface. The heat slowly excites electrons across the AZO, reducing its conductivity (as seen from the charging portion of the top graph in Fig. 4). When contact is made with the node, there is a discharge of electrons across the channel that can be noticed from the immediate increase in current from the top plot of Fig. 4. Also seen from the top plot of Fig. 4 is a gradual reduction in conductivity until pressure is released, a behavior explained by charge accumulation before contact.

Heating the parallel plate structure of the silver routing pattern before contact causes a capacitive charging behavior, where electrons gradually collect at the plates. After making contact, the current spikes and the accumulated charge dissipates slowly before reaching an equilibrium current. When pressure is released with no additional heat exposed to the sensor, the node slowly discharges. This charge/discharge feature is only barely noticeable in the constant pressure profile of Fig. 3 because there was little to no charge before contact. The bottom plot of Fig. 4 has charging regions where the heat source (index finger) was placed 1 mm above the surface of a node to heat it and accumulate charge. Greater charging before contact resulted in higher current output of equally applied pressures as indicated in Fig. 4.

2) Application Viability: This sensor's implementation as a foot pressure mapping element for physical therapy was tested for a single node to further explore its charging behavior in the application domain. Fig. 5 shows the response of a single node when various movements were performed such as sitting, standing, and walking. The pressures applied during these tests was up to 26.9 PSI, as calculated by the weight imposed

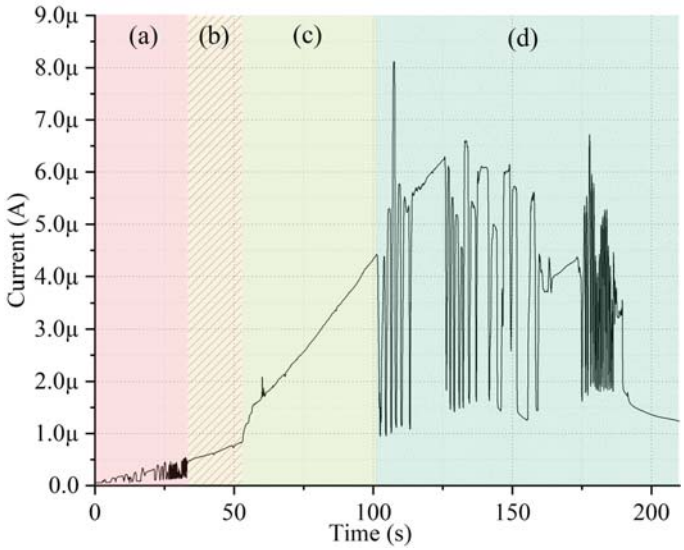

Fig. 5: Current response when various weight is applied to node a_{11}. Supply voltage is 5V with a max pressure of 130 pounds (i.e. approximately the weight of a human). Pressures are as follows: (a) varying pressures without pre-charge by the foot, (b) foot pressure from sitting, (c) foot pressure from standing and (d) is random foot pressures after pre-charge.

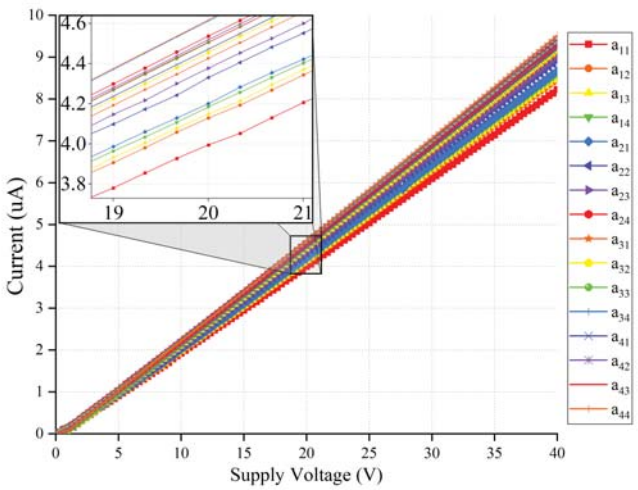

Fig. 6: I-V curves of the pressure array nodes. Print variability causes inconsistent slopes at each node.

through the foot (135 lb) divided by surface area of the heel touching the sensor (5.02 in^2). Heat from the foot transfers to the sensor, gradually increasing its current output (i.e. charging) under constant pressure while sitting and standing (parts (b) and (c) of Fig. 5, respectively). Fig. 5 (d) shows that the current variations after it has been charged from sitting or standing is much greater than when the same pressures were applied before the charging effect was imposed on the node as seen in Fig. 5 (a). Thus, the nodes will charge when the user is not moving and will have an increasing/decreasing average when walking or running, depending on the heat output of the foot. This forms a link for calibrating pressure and classifying the movements at each node, thus forming the desired mapping function. The rate of output current changes when standing or sitting, coupled with a thermostat to cross-reference the user's temperature at the foot would be used to validate the relationship between output signal and thermal exposure.

3) Calibration: Pressure calibration of this sensor begins with mapping the range of output current to the known applied pressures. The maximum pressure applied during these tests was 540 PSI as calculated from the maximum weight applied by the finger (14 lb) divided by the area of pressure application to the node (0.0259 in^2). The maximum output seen from Fig. 3 is 10 μA, making the ratio of PSI-to-power output equal 2.7 PSI/μW. The same calculation was made with the uncharged region of Fig. 5 (portion (a) of the figure). The maximum output current is approximately 500 nA for a power output of 2.5μW, and with the foot pressure of 26.9 PSI the ratio is 10.8 PSI/μW. The PSI-to-power ratio can be used during data processing to calibrate the applied PSI of uncharged nodes.

All of these findings indicate that the node's current response can be mapped to pressure regardless of the supply voltage value or applied force, making the single node compatible as a system-level sensing device. Changes in heat and humidity alters the calibration ratio, giving sensing ability to those variables.

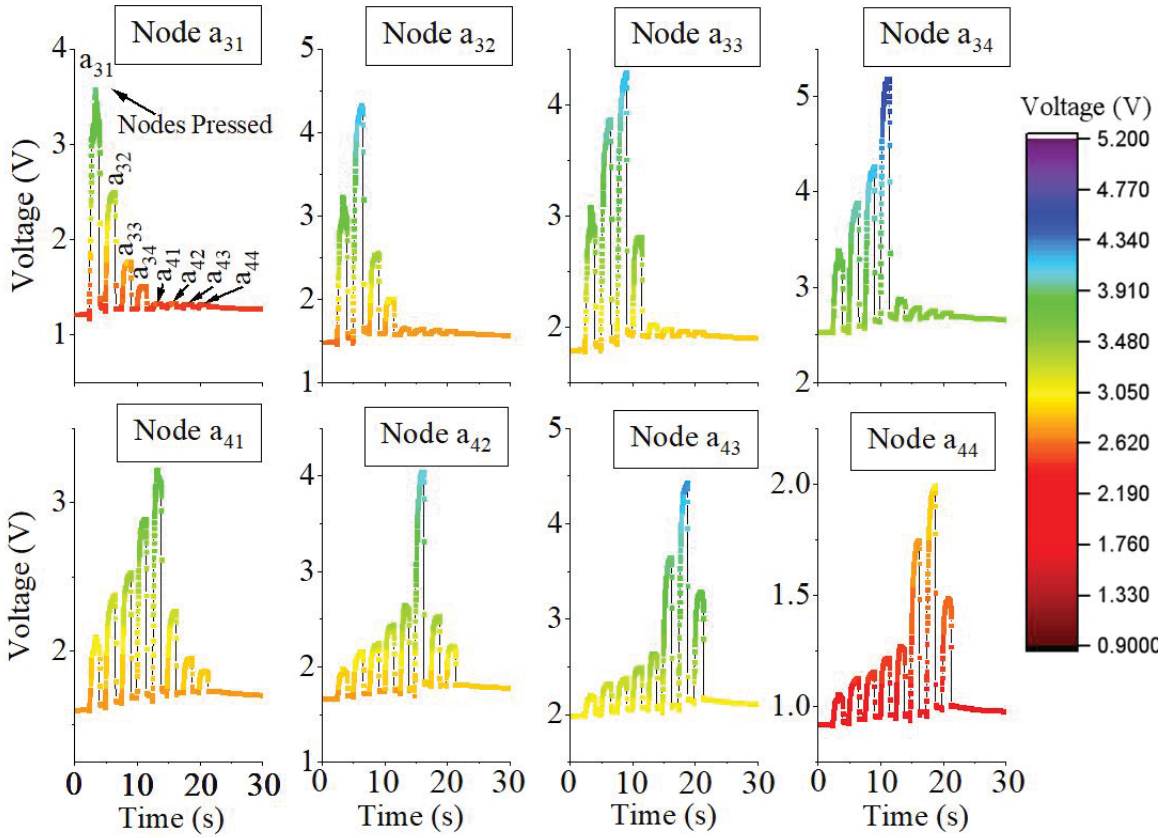

Fig. 7: Single pressure point response of nodes a_{31} through a_{44} (the second eight nodes) with color scale. Note that rows are more dependent with each other than columns and each node exhibits independent scales of response.

4) System-Level Considerations: In order to understand the viability of this sensor as an input to system-level designs, the variability of electrical behavior among the nodes was explored. Inkjet printers output slightly variable prints and with uneven curing, differences between identical samples complicates the ability standardize all nodes for processing as a single unit. These differences can be seen from the zoomed in region of the IV curve (Fig. 6), where the curves for each node are not identical. Fig. 7 is the generated output of 8 nodes from the array, observed at the same time. Note that each node is slightly biased at a different voltage, and their maximum amplitudes are not the same. Thus, each node must be standardized according to the calibration settings at the beginning of data acquisition. This plot also shows that each node has its highest amplitude when touched, meaning that the node with the greatest amplitude at any given time (after being standardized) indicates which node was pressed. There is an outlier with node a_{44} as it does not indicate the correct node being pressed, and that goes to show how inconsistency of the print effects total functionality. The top four sub-plots of Fig. 7 are all on the same row of the array (third row), while the second four sub-plots are all on the fourth row. The voltage output of nodes along the columns show good sensor selectivity. However, nodes show more dependence along the rows and reduces the pressure mapping resolution. The geometry will be considered for system-level designs.

IV. Conclusion

The low-cost, flexible printed pressure array sensor explored in this report was shown to exhibit a range of behaviors resulting from its geometry, materials, printing/curing consistency, and heat/humidity conditions. The maximum pressure applied (540 PSI) was easily sensed and after cross-validating tests, calibration ratios comparing PSI to power output was calculated for uncharged samples. Charging effects occur when a heat source is within 4 mm of the node, adding a temperature-sensing variable to the pressure sensor. Evaluating the output signal's rate of change and PSI/μW differences during charging gives insight to the user's thermal conditions. These parameters will be standardized for each node during signal pre-conditioning since the printed nodes are not entirely identical. Future work will include this sensor integrated with a signal processing scheme for proof-of-concept as a human-touch pressure mapping sensor. The calibration settings will be evaluated for reliability during operation and critical parameters such as sample lifetime, node variability, and print geometry will be refined for improved responses. This inkjet-printed sensor will one day provide a method of ultra-inexpensive pressure mapping for topics including physical training, mobility monitoring and human impact studies.

REFERENCES

[1] J. Szałatkiewicz, "Metals content in printed circuit board waste," *Polish Journal for Environmental Studies*, vol. 23, no. 6, pp. 2365–2369, 2014.

[2] J. S. Chang, A. F. Facchetti, and R. Reuss, "A circuits and systems perspective of organic/printed electronics: Review, challenges, and contemporary and emerging design approaches," *IEEE Journal on Emerging and Selected Topics in Circuits and Systems*, vol. 7, no. 1, pp. 7–26, 2017.

[3] M. Singh, H. M. Haverinen, P. Dhagat, and G. E. Jabbour, "Inkjet printing - process and its applications," *Polish Journal for Environmental Studies*, vol. 22, pp. 673–685, 2010.

[4] E. R. Garcia, "Inkjet printed microelectronic devices and circuits (doctoral dissertation)," *Universitat Autonoma de Barcelona*, 2014.

[5] M. Myllys, H. Häkkänen, and K. Korppi-Tommola, "X-ray microtomography and laser ablation in the analysis of ink distribution in coated paper," *Journal of Applied Physics*, vol. 117, no. 144902, 2015.

[6] B. D. Paulsen, A. Giovannitti, V. Venkatraman, and J. Rivnay, "Organic bioelectronic materials and devices for bridging biology and traditional electronics," *Material Matters*, vol. 14, no. 1, pp. 3–7, 2019.

[7] G. C. Marques, F. Rasheed, J. Aghassi-Hagmann, and M. B. Tahoori, "From silicon to printed electronics: A coherent modeling and design flow approach based on printed electrolyte gated fets," in *2018 23rd Asia and South Pacific Design Automation Conference (ASP-DAC)*, Conference Proceedings, pp. 658–663.

[8] F. Maldonado and A. Stashans, "Al-doped zno: Electronic, electrical and structural properties," *Journal of Physics and Chemistry of Solids*, vol. 71, no. 5, pp. 784–787, 2010.

[9] B. Hussain, M. Y. A. Raja, N. Lu, and I. Ferguson, "Applications and synthesis of zinc oxide: An emerging wide bandgap material," in *2013 High Capacity Optical Networks and Emerging/Enabling Technologies*, Conference Proceedings, pp. 88–93.

[10] L. Kou, W. Guo, and C. Li, "Piezoelectricity of zno and its nanostructures," in *2008 Symposium on Piezoelectricity, Acoustic Waves, and Device Applications*, Conference Proceedings, pp. 354–359.

[11] A. Bierbaum, "Zinc oxide nanoparticles: doping, inkjet printing, and electron accepting from photoexcited porphyrin dyes," *Retrieved from the University of Minnesota Digital Conservancy*, 2013.

[12] Y. N. Liang, B. K. Lok, and X. Hu, "Spatially selective patterning of zinc oxide precursor solution by inkjet printing," in *2009 11th Electronics Packaging Technology Conference*, Conference Proceedings, pp. 174–179.

[13] L. J. Hoong, Y. C. Keat, A. Chik, and T. P. Leng, "Band structure and thermoelectric properties of inkjet printed zno and znfe2o4thin films," *Ceramics International*, vol. 42, no. 10, pp. 12 064–12 073, 2016.

[14] D. Inamdar, C. Agashe, P. Kadam, and S. Mahamuni, "Doping optimization and surface modification of aluminum doped zinc oxide films as transparent conductive coating," *Thin Solid Films*, vol. 520, no. 11, pp. 3871–3877, 2012.

[15] K. Vernieuwe, "Synthesis of aqueous inks for the deposition of al doped zno thin films and patterns," *Department of Inorganic and Physical Chemistry*, 2015.

[16] A. Sacramento, M. Ramírez-Como, V. S. Balderrama, S. I. Garduño, M. Estrada, and L. F. Marsal, "Degradation study of inverted polymer solar cells using inkjet printed zno electron transport layer," in *2019 Latin American Electron Devices Conference (LAEDC)*, vol. 1, Conference Proceedings, pp. 1–4.

[17] Y. Wu, T. Tamaki, W. Voit, L. Belova, and K. V. Rao, "Ultraviolet photoconductivity of pure and al doped zno thin films by inkjet printing," in *2009 MRS Spring Meeting, April 14, 2009 - April 17, 2009*, ser. Materials Research Society Symposium Proceedings, vol. 1183. Materials Research Society, Conference Proceedings, pp. 133–138.

[18] S. Gardner, M. R. Haider, M. T. Islam, J. I. D. Alexander, and Y. Massoud, "Aluminum-doped zinc oxide (zno) inkjet-printed piezoelectric array for pressure gradient mapping," *62nd IEEE International Midwest Symposium on Circuits and Systems*, 2019.

[19] S. Kim, M. Amjadi, T. Lee, Y. Jeong, D. Kwon, M. S. Kim, K. Kim, T. Kim, Y. S. Oh, and I. Park, "Wide range-sensitive, bending-insensitive pressure detection and application to wearable healthcare device," in *2019 20th International Conference on Solid-State Sensors, Actuators and Microsystems & Eurosensors XXXIII (TRANSDUCERS & EUROSENSORS XXXIII)*, Conference Proceedings, pp. 374–377.

[20] J. R. Greer and R. A. Street, "Thermal cure effects on electrical performance of nanoparticle silver inks," *Acta Materialia*, vol. 55, no. 18, pp. 6345–6349, 2007.

[21] Y. Li, M. R. Haider, and Y. Massoud, "An efficient orthogonal pulse set generator for high-speed sub-ghz uwb communications," in *2014 IEEE International Symposium on Circuits and Systems (ISCAS)*, Conference Proceedings, pp. 1913–1916.

[22] Y. Li, Q. Ma, M. R. Haider, and Y. Massoud, "Ultra-low-power high sensitivity spike detectors based on modified nonlinear energy operator," in *2013 IEEE International Symposium on Circuits and Systems (ISCAS)*, Conference Proceedings, pp. 137–140.

[23] M. S. E. Quadir, M. R. Haider, and Y. Massoud, "A low-power low-noise bioamplifier for multielectrode neural recording systems," in *2012 IEEE International Symposium on Circuits and Systems (ISCAS)*, Conference Proceedings, pp. 2557–2560.